Biosensors and Bioelectronics 77 (2016) 853–859

Contents lists available at ScienceDirect

Biosensors and Bioelectronics

journal homepage: www.elsevier.com/locate/bios

A switched catalysis qualified sealers capped one-step synthesis biocompatibility bimetallic scaffold film for Neu5Acα(2-6)Gal β MP Glycoside specific detection

Chunyong Xia [1], Junlin He [1], Guolin Yuan, Yuliang Li, Qingying Li, Chao Yu *

Institute of Life Science and School of Public Health, Chongqing Medical University, Box 174#, No. 1 Yixueyuan Road, Chongqing 400016, PR China

ARTICLE INFO

Article history:
Received 5 August 2015
Received in revised form
16 October 2015
Accepted 21 October 2015
Available online 23 October 2015

Keywords:
Neu5Acα(2-6)Gal β MP Glycoside
AuPt–PPy
Glucose oxide
Electrochemical catalytic

ABSTRACT

In this work, a novel label-free biosensor was designed for the sensitive and selective determination of Neu5Acα(2-6)Gal β MP Glycoside using AuPt–PPy(polypyrrole) conductive nanocomposite film as the sensor platform. The introduced AuPt–PPy nanocomposite provided a large surface area for the immobilization of *Sambucus nigra agglutinis* (SNA) through a coupling agent for specifically recognizing analytes and exhibited high electrocatalytic activity toward the reduction of hydrogen peroxide (H_2O_2) as an analytical signal. Subsequently, to block the non-specific sites of the modified electrode, GOx was employed instead of the usual sealers. Most importantly, in the presence of glucose, these localized GOx further enhanced the electrochemical signal, which was achieved by the efficient catalysis of glucose. This study is the first that demonstrates the specific detection of Neu5Acα(2-6)Gal β MP Glycoside using AuPt–PPy as the electrocatalytic. Under optimal conditions, the electrochemical biosensor exhibited a wide linear range of 0.01 pg mL^{-1}–800 ng mL^{-1} with a low detection limit of 0.003 pg mL^{-1} ($S/N=3$), due to the affinity between SNA and Neu5Acα(2-6)Gal β MP Glycoside. Therefore, the co-catalysis signal amplification approach has considerable potential in clinical applications and is suitable for the quantification of other biomarkers.

1. Introduction

Glycosylations, or the alternations of cell surface glycan structures, are dynamic and stage-specific processes. There is accumulating evidence for the role of glycans in cell adhesion, fertilization, differentiation, and development (Matsumoto et al., 2009; Raman et al., 2005; Wang et al., 2003). Sialic acid (SA), also known as N-acetylneuraminic acid (Neu5Ac), is an anionic monosaccharide that frequently occurs at the terminal of the glycan chains (Gao et al., 2014). The α2,6-linkage of sialic acids on N-acetyllactosamine structure (Galβ1–4GlcNAc), which is important in cell–cell and cell–matrix interactions (Kim et al., 2006), is catalysed by enzymes of the sialytransferase (ST) family (Harduin-Lepers et al., 2001; Park et al., 2012). Accumulating evidence demonstrate that over-expression of the sialyation on a cell surface is closely associated with the development and progression of certain cancers, such as breast cancer (Recchi et al., 1998), colorectal cancer (Dall'Olio et al., 1999) and hepatocellular cancer (Pousset et al., 1997). Therefore, monitoring the α2,6-sialylated glycan changes in serum as crucial molecular targets is notably important for cancer diagnoses. Nowadays, alternative technologies to classic methods are under development, including gas chromatography–mass spectrometry, capillary electrophoresis (Bratosin et al., 2007; Bugla-Ploskonska et al., 2010; Kim et al., 2006), and nuclear magnetic resonance spectroscopy (Hobb et al., 2010; Jones 2005). Nevertheless, these latter technologies typically require time-consuming and expensive instruments. In particular, they cannot meet the clinical demand of early-stage detection. Therefore, it is necessary to explore a novel and facile method for detection of Neu5Acα(2-6)Gal β MP Glycoside in serum.

Bimetallic nanoparticles (NPs) with intrinsic peroxidase-like activity have been widely used in many applications and exhibit perfect catalytic performance (Bai et al., 2011). For bimetallic NPs, one metal can take on a long-term stability and biocompatibility, and the other could provide the specific electrical activity, including electrochemical catalytic activity (Chen et al., 2012). Recently, AuPt bimetallical NPs have been widely used in electronic fields due to their high catalytic activity, excellent biocompatibility and good stability. For example, AuPt bimetallic NPs have been reported to develop a novel immunosensor for the detection of

* Corresponding author. Fax: +86 23 68486294.
E-mail address: yuchaom@163.com (C. Yu).
[1] These two authors contributed equally to this work.

http://dx.doi.org/10.1016/j.bios.2015.10.060
0956-5663/

carcinoembryonic antigen (CEA), in which the combination of AuPt bimetallic NPs with graphene-nanotubes was used for signal amplification (Cao et al., 2013). Conducting polymers (CPs), such as polypyrrole (PPy), with the advantage of low density, facile synthesis, high electrical conductivity, and mechanical integrity, have been widely used in the field of electrochemical sensing (Ahuja et al., 2007; Hu et al., 2008; Lee et al., 2006; Lin et al., 2012). Considering the benefits of the above two materials, the integration of AuPt bimetallic NPs and PPy have been prepared according to the reported method (Wang et al., 2013). More importantly, the AuPt–PPy nanocomposite has high electrocatalytic activity. However, no known research is available that focuses on AuPt–PPy as an electrocatalytic application for electrochemical biosensors.

AuPt–PPy nanocomposite, synthesized through sequential reduction by utilizing Py monomer as a reducing agent and a weak ligand protection (Wang et al., 2013), shows higher electrocatalytic activity toward H_2O_2 reduction. Considering this property of AuPt–PPy, this study demonstrates that AuPt–PPy is ideal material for use in electrochemical biosensors as a catalytic matrix.

In this work, a novel label-free biosensor for Neu5Acα(2-6)Gal β MP Glycoside is presented, based on glucose oxide (GOx) and the electrocatalytic activity of AuPt–PPy. Firstly, AuPt–PPy served as the electrochemical signal by efficient catalysing H_2O_2, and it served as carrier to load *Sambucus nigra agglutinis* (SNA) and GOx. Recently, SNA was used as an excellent candidate for biosensor fabrication, because of its highly specific binding affinity with α2,6-sialylated glycans (Cao et al., 2015; Chen et al., 2007; Shoji and Freund, 2002; Zhou et al., 2014). Subsequently, in the presence of glucose the carried GOx catalysed the oxidation of glucose; the electrochemical responses were enhanced. In the process of Neu5Acα(2-6)Gal β MP Glycoside detection, hydrogen peroxide is initially reduced by the prepared AuPt–PPy nanocomposite, thus the produced oxygen can assist the oxidization of glucose in the presence of GOx. The electrochemical signals were obtained under the co-catalysis effect. According to the measurement principles, the Neu5Acα(2-6)Gal β MP Glycoside in the serum samples could be determined.

2. Materials and methods

2.1. Reagents and chemicals

$HAuCl_4 \cdot 3H_2O$, $H_2PtCl_6 \cdot 6H_2O$, pyrrole (Py, 98%), Sodium 1-dodecanesulfonate (SDS, 99%), Glutaraldehyde (GA) and Glucose oxidase (GOx) were purchased from Sigma Aldrich (St. Louis, USA, www.sigmaaldrich.com). Neu5Acα(2-6)Gal β MP Glycoside was purchased from Tokyo Chemical Industry (Japan, www.TCIchemicals.com, Lot. SGPSH-HF, > 98%). *Sambucus nigra agglutinin* was purchased from Gentaur (Kampenhout, Belgium, www.gentaur.com). Hydrogen peroxide (H_2O_2, 30%) was obtained from the Chongqing Chuandong Chemical Company (China, www.cqchemgroup.com).

Ferricyanide solutions ($Fe(CN)_6^{3-/4-}$, 10.0 mM) were obtained by dissolving potassium ferricyanide and potassium ferrocyanide with de-ionized distilled water. Phosphate buffer solutions (PBS) (0.1 M) were prepared using 0.1 M Na_2HPO_4 and 0.1 M KH_2PO_4. All reagents were of analytical grade and were used without further purification. All aqueous solutions were prepared with de-ionized distilled water (resistivity > 18 MΩ cm, USA, www.millipore.com) obtained from a Milli-Q water purifying system.

2.2. Apparatuses

Cyclic Voltammograms (CVs), amperometric *i–t* curve and differential pulses voltammograms (DPV) were recorded using a model 660D electrochemical workstation (Chenhua Instruments Co., Shanghai, China). Scanning electron microscope (Model Hitachi-7500158, Hitachi Limited, Japan) and Transmission electron microscope (TEM) images were also obtained from the same equipment model and company. Energy dispersive X-ray Spectroscope (EDS) measurements were obtained with a JROL JSM-6700F microscope (Japan). Atomic force microscope (AFM) images were obtained with a Bruker Dimension Icon microscope (USA).

2.3. Preparation of AuPt–PPy composite

The AuPt–PPy was synthesized by a typical synthesis method. Briefly, 4 μL of distilled Py monomer was mixed with 2 mL of SDS aqueous solution (8.27 mM), followed by stirring for 2 h to obtain a uniform solution. Afterward, H_2PtCl_6 (0.3 mL, 5%) and $HAuCl_4$ (0.5 mL, 1%) were added into the solution. The obtained mixture was gently stirred for 24 h at 50 °C. The AuPt–PPy composites were separated by centrifugation (12000 rpm for 15 min) and later washed with the ultrapure water and ethanol several times to remove residual Py. The resulting precipitate was dispersed again in 2.5 mL distilled water and stored at 4 °C prior to use.

The Au–PPy ($HAuCl_4$, 0.5 mL, 1%) and Pt–PPy (H_2PtCl_6, 0.3 mL, 5%) samples were also prepared with similar procedures.

2.4. Fabrication of the biosensor

The preparation process of the biosensor is displayed in Scheme 1. Glassy carbon electrodes (GCE, diameter 5.0 mm) were used as the substrates for modification with the prepared AuPt–PPy nanocomposite and GOx. Before modification, the GCE was polished with 0.3 and 0.05 μm alumina powder, followed by successive sonication with ethanol and double-distilled water in an ultrasonic bath for 5 min. Subsequently, 4 μL of AuPt–PPy dispersion was dropped on the surface of the prepared GCE and left to dry at room temperature. To attach the lectin, SNA, freshly prepared glutaraldehyde (GA) solution (2.5%, 4 μL) was added to the substrate, followed by incubation for 2 h at room temperature. In the reaction process, the solution of SNA and PPy reacted with GA, forming a Schiff base structure (Cete et al., 2007; Cozzi 2004; Rover Junior et al., 2000). After absolutely washing with distilled water, the obtained electrode was incubated in 1 μg mL^{-1} SNA at room temperature for 40 min. Next, the electrode was carefully washed with PBS (pH = 7.4) to remove excessive SNA. Finally, 20 μL of GOx (1 mg mL^{-1}) solution was dropped on the modified electrode surface and incubated at 4 °C to block the non-specific binding sites. After washing thoroughly with pH 7.4 PBS, the prepared electrode was stored at 4 °C prior to use.

2.5. Measurement of procedure

All electrochemical measurements were performed by a standard three-electrode system: a glass carbon electrode as the working electrode, a saturated calomel electrode (SCE) as the reference electrode and a platinum wire electrode as the counter electrode. The electrochemical detection was performed in 5 mL of PBS at room temperature by amperometric *i–t* curve with int $E = -0.4$ V. After the background current was stabilized, 20 μL of PBS solution containing 1 mol L^{-1} H_2O_2 and 1 mg mL^{-1} glucose was added into the butter, and recordings were subsequently made of the current change.

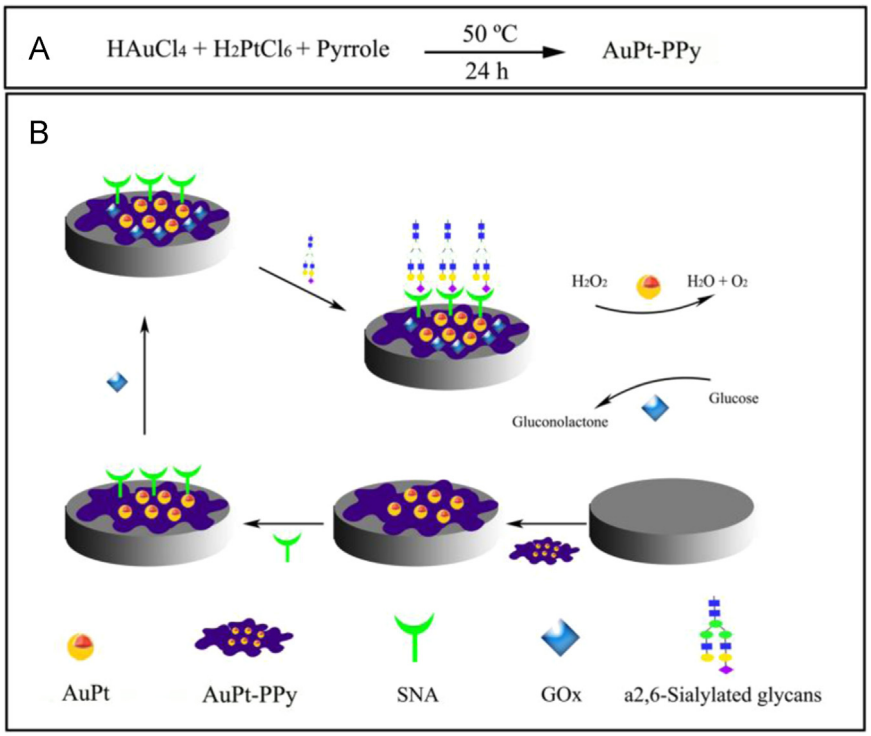

Scheme 1. Schematic diagrams for (A) the synthesis procedure of AuPt–PPy nanocomposite, and (B) the fabrication procedure of the electrochemical biosensor.

3. Results and discussion

3.1. Characterization of materials

The size and morphology changes of AuNPs, AuPtNPs and AuPt–PPy were characterized by TEM (Fig. 1). Fig. 1A displays the typical TEM image of AuNPs, dense and uniform AuNPs with sizes of approximately 10 nm were observed. The AuPt bimetallic nanocomparticles are shown in Fig. 1B, and the AuPtNPs consists of chained nanoparticles with sizes of approximately 18–20 nm, which owns much larger size than single AuNPs. Furthermore, compared with the AuNPs, the structure of the AuPt bimetallic nanocomparticles have darker color. Fig. 1C shows the TEM image of AuPt–PPy obtained by a facile one-pot reaction. It is clearly observed that a large amount of AuPt nanoparticles with an average size of approximately 20 nm are successfully embedding in the PPy film. To demonstrate further the successful synthesis of AuPt–PPy, the corresponding energy dispersive spectroscopy (EDS) of AuPt–PPy is given in Fig. 1C. It is clear that the intensity of the Pt peak is higher than that of Au, indicating that Pt is focused outside the gold particles. In addition, obvious C and N peaks were performed to confirm the existing of PPy. The EDS and TEM images shown in Fig. 1C confirm that the AuPt–PPy nanocomposite film was synthesized successfully.

To obtain more evidence to confirm the successful immobilization of SNA on the nanocomposite film surface successfully, atomic force microscopy (AFM) was used to investigate the bioconjugation process. Fig. 2 shows the three dimensional (a) and cross-sectional (b) images of AuPt–PPy/GCE (A) and SNA/GA/AuPt–PPy/GCE (B). By comparison, the AuPt–PPy/GCE is relatively flat and smooth, with the greatest peak height being 15.795 nm (Fig. 2A). The average roughness (Ra) was determined to be 2.14 nm. After the immobilization of SNA on the AuPt–PPy/GCE through the coupling agent, the peak height was approximately 32.784 nm, due to the aggregation of SNA on the nanocomposite. The surface roughness increased to 6.84 nm (Fig. 2B). These surface changes demonstrated the feasibility of nanocomposite and biomolecule self-assembly via coupling agent bioconjugation.

For an electrochemical biosensor, signal amplification is critical to obtain high sensitivity and a low detection limit. In this study, the electrocatalytic signal of the biosensor is based on the high electrocatalytic activity of AuPt–PPy for the reduction of H_2O_2 and GOx for the efficient catalysis of glucose. For comparison purposes, the catalytic performances of Au–PPy, Pt–PPy, AuPt–PPy toward

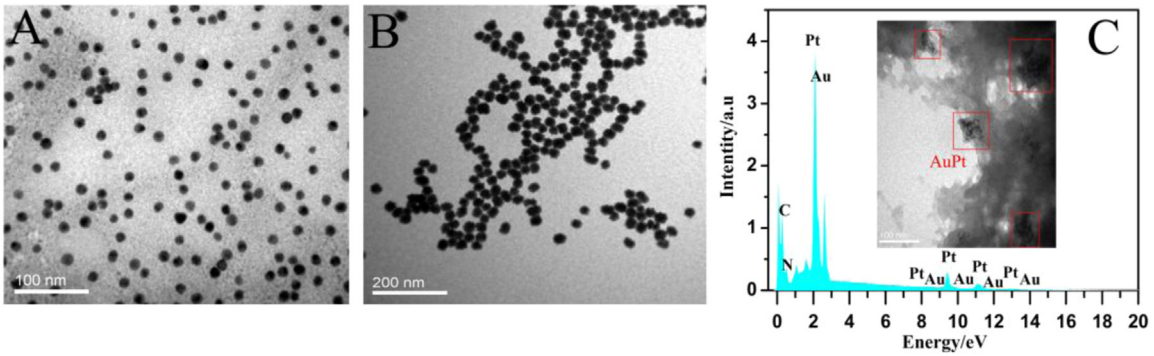

Fig.1. TEM images of (A) AuNPs, (B) AuPtNPs, (C) EDS and TEM of AuPt–PPy nanocomposite.

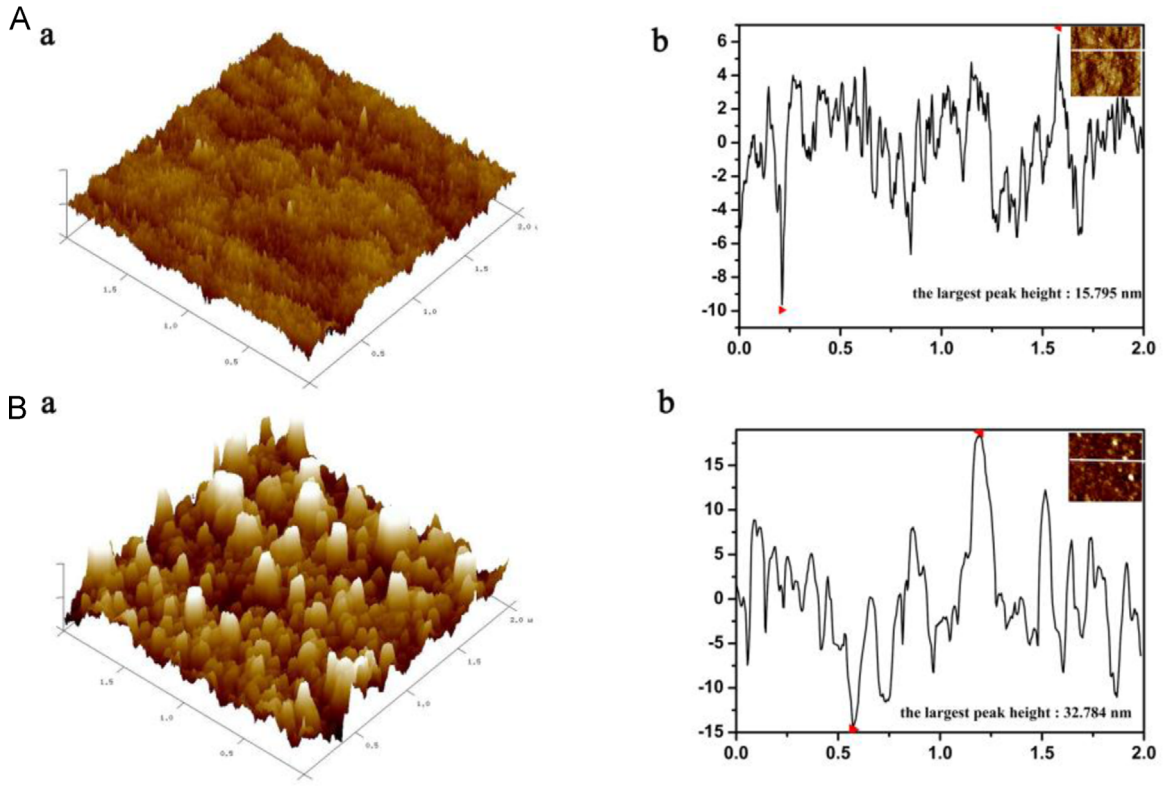

Fig. 2. AFM images of (a) three dimensional and (b) cross-sectional graphs of (A) AuPt–PPy and (B) SNA/GA/AuPt–PPy.

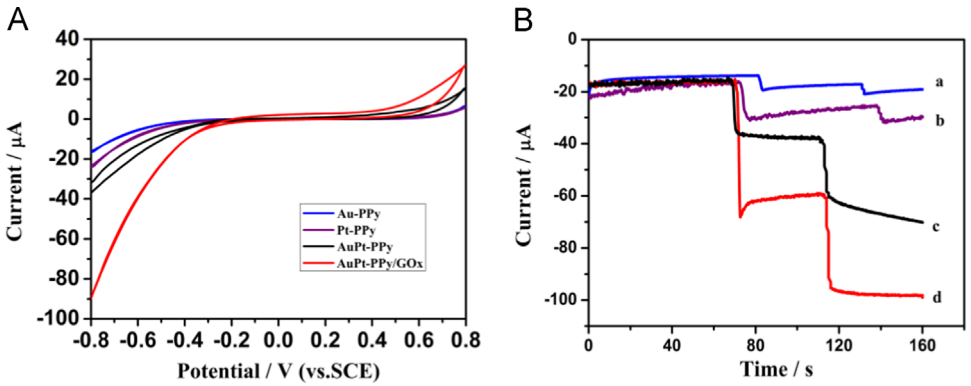

Fig. 3. (A) The respective electrocatalytic ability of Au–PPy, Pt–PPy, AuPt–PPy and AuPt–PPy/GOx in 1 mol L^{-1} H_2O_2 containing 1 mg mL^{-1} glucose. (B) Amperometric response of the modified electrodes with Au–PPy (a); Pt–PPy (b); AuPt–PPy (c) and AuPt–PPy/GOx (d) toward successive addition of 1 mol L^{-1} H_2O_2 containing 1 mg mL^{-1} glucose in PBS (pH=7.4).

H_2O_2 were investigated. The signal responses of the biosensor prepared with different metal particles and Py monomer toward H_2O_2 are shown by the cyclic voltammetry (Fig. 3A). It was obvious that AuPt–PPy modified GCE will have better catalytic properties toward H_2O_2 than any monometallic electrode. In this study, AuPt–PPy was selected as catalytic matrix of the biosensor. Furthermore, the use of GOx/AuPt–PPy bioconjugate displayed the highest current change toward H_2O_2 in the presence of glucose, suggesting the GOx could extremely enhance the electrochemical signal by the efficient catalysis of glucose. Meanwhile, as shown in Fig. 3B, the amperometric *i–t* curve further supported the above conclusion.

3.2. Characterization of the biosensor fabrication

The biosensor fabrication process was investigated by recording cyclic volyammograms (CVs) of the modified electrode in 10 mM $Fe(CN)_6^{3-/4-}$ solution containing 0.1 M KCl during the preparation steps (Fig. S1A). A reversible redox response was observed at the bare electrode (curve a). After the AuPt–PPy modified electrode, an obviously increased peak current was found (curve b). This result suggested that AuPt–PPy promoted electron transfer and enhanced the conductivity of the electrode. The accessible active surface area *A* of AuPt–PPy modified electrode and the bare electrode could be calculated through the CVs results displayed in Fig. S1A, according to the following Randles–Sevcik equation (Li et al., 2015; Zheng et al., 2014):

$$I_{pc} = (2.69*10^5)n^{3/2}AD^{1/2}Cv^{1/2}$$

The values of *A* for the bare GCE and the AuPt–PPy modified electrode were calculated as 32.21 and 47.08 mm^2, respectively, which demonstrated that AuPt–PPy increased the accessible area of the electrode roughly 1.5-fold. When the modified electrode

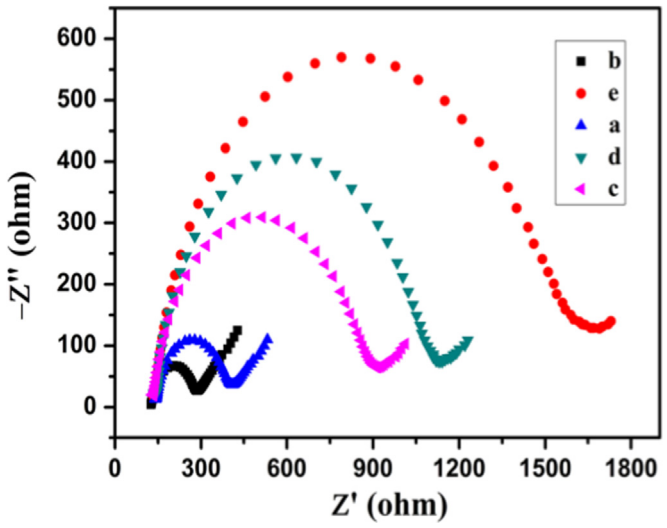

Fig. 4. The EIS of different electrodes performed in 10 mM $Fe(CN)_6^{3-/4-}$ solution containing 0.1 M KCl: (a) bare electrode, (b) AuPt–PPy/GCE, (c) SNA/GA/AuPt–PPy/GCE, (d) GOx/SNA/GA/AuPt–PPy/GCE, and (e) Neu5Acα(2-6)Gal β MP Glycoside/GOx/SNA/GA/AuPt–PPy/GCE. The scan rate was 50 mV s^{-1}, and all potentials were given versus SCE.

was incubated with SNA, the peak current obviously decreased for the SNA protein, acting as a mass transfer block and hindering the diffusion of ferricyanide toward the electrode surface (curve c). The peak current continued to decrease after the incubation of both GOx (curve d) and Neu5Acα(2-6)Gal β MP Glycoside (curve e).

The impedance changes of the electrode surface during the electrode modification process could be observed from the semicircle portion changes of the electrochemical impedance spectroscopy (EIS) at high frequencies. As shown in Fig. 4, the semicircle associated with the GCE modified with AuPt–PPy composite film (curve b, R_{et}=141 Ω) was smaller than that associated with the bare GCE (curve a, R_{et}=307.3 Ω) due to the comprehensive properties of the materials. The charge transferring resistance (R_{et}) values at the SNA modified electrodes increased obviously (curve c, R_{et}=792.2 Ω), which suggested that the SNA was successfully immobilized on the surface, formed an additional barrier and blocked the electron exchange between the redox probe and the electrode. Similarly, R_{et} further increased with the addition of GOx (curve d, R_{et}=994.5 Ω) and Neu5Acα(2-6)Gal β MP Glycoside (curve e, R_{et}=1476 Ω), indicating that the formed complex blocked the electron transfer. These results were in accordance with the changes observed by the CVs. Additionally, differential pulse voltammetry (DPV) was also performed to monitor the fabrication process of the stepwise biosensor. As shown in Fig. S1B, the DPV results were consistent with the CVs and EIS. These measurements indicate the successful stepwise assembly of the biosensor.

To investigated further the electrochemical behavior, CVs studies were conducted at different scan rates (30–500 mV/s) in a 10 mM $Fe(CN_6)^{3-/4-}$ solution containing 0.1 M KCl. As shown in Fig. S2, a linear relationship was found between the peak current I_p (both I_{pa} and I_{pc}) and the square root of the scan rate. The linear regression equation was I_{pa} (μA)=21.434+12.378$\nu^{1/2}$ (R^2=0.9995) and I_{pc} (μA)=−46.002−8.463$\nu^{1/2}$ (R^2=0.9840). Based on the above results, it could be demonstrated that the electrochemical reaction at electrode surface was a diffusion-controlled process (Che et al., 2011; Gomes-Filho et al., 2013; Zhang et al., 2011).

3.3. Optimization of experimental conditions

To obtain the best analytical performance for Neu5Acα(2-6)Gal

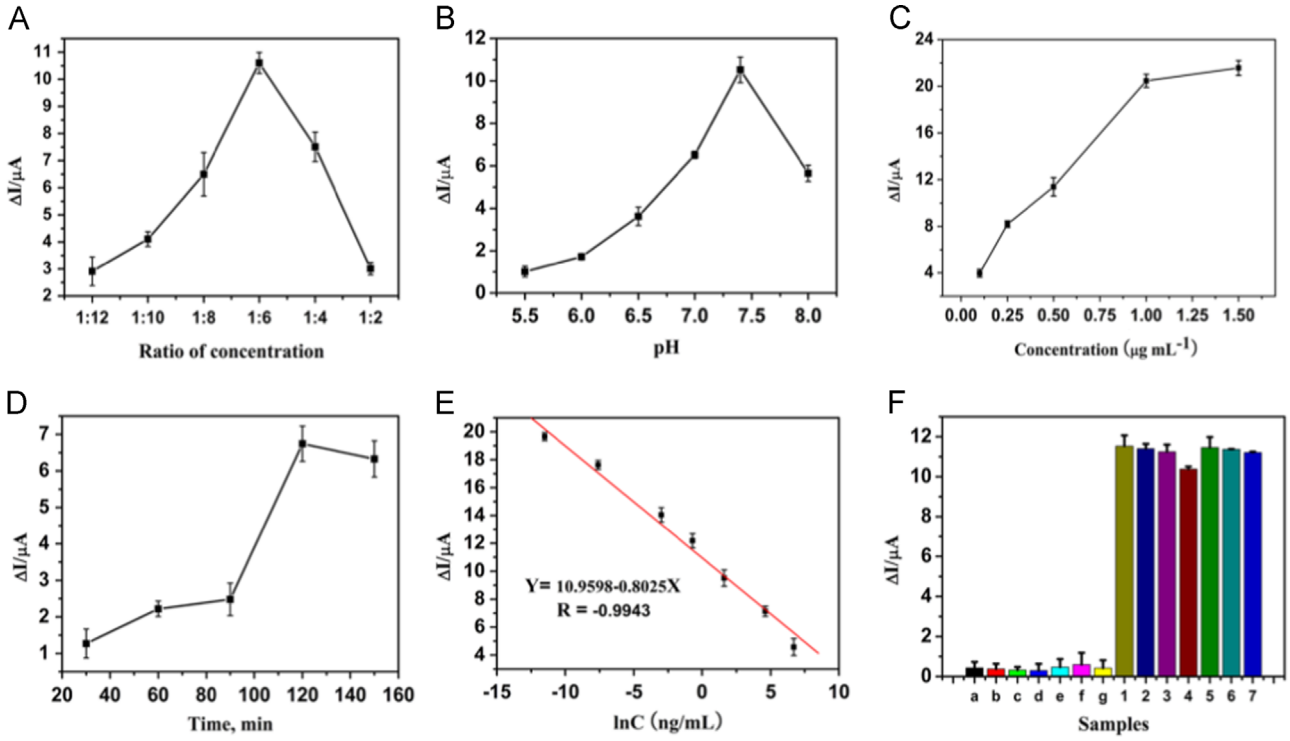

Fig. 5. Effect of (A) the concentration of AuPt–PPy,(B) pH of working buffer, (C) concentration of SNA and (D) the incubation time of the receptor/ligand. (E) Calibration curve of the biosensor toward different concentrations of Neu5Acα(2-6)Gal β MP Glycoside. (F) The selectivity of the proposed biosensor for α2,6-sialylated glycans detection was examined by comparing it with different interfering substances: (a) blank, (b) 1 μg mL^{-1} AA, (c) 1 μg mL^{-1} BSA, (d) 1 μg mL^{-1} hs-CRP, (e) 1 μg mL^{-1} L-cysteine, (f) 1 μg mL^{-1} ST6GAL1, (g) 1 μg mL^{-1} Glu, (1) 1 ng mL^{-1} analyte, (2) 1 ng mL^{-1} analyte+1 μg mL^{-1} AA, (3) 1 ng mL^{-1} analyte+1 μg mL^{-1} BSA, (4) 1 ng mL^{-1} analyte+1 μg mL^{-1} hs-CRP, (5) 1 ng mL^{-1} analyte+1 μg mL^{-1} L-cysteine, (6) 1 ng mL^{-1} analyte+1 μg mL^{-1} ST6GAL1, (7) 1 ng mL^{-1} analyte+1 μg mL^{-1} Glu.

β MP Glycoside, the detection conditions of the experiment were optimized.

The ratio of concentration of AuPt–PPy for preparation of the biosensor was an important parameter affecting the signal responses. The effect of different ratios concentrations of AuPt–PPy on the current change (ΔI) are shown in Fig. 5A. It was found that ΔI values increase rapidly when increasing the ratio of concentration from 1:12 to 1:6, the values later decreased at 1:4 ratio. This finding might be attributed to the further increase of AuPt–PPy thickness that blocked the electron transfer on the surface of electrode. Hence, the optimal ratio concentration of AuPt–PPy was achieved at 1:4.

The pH of the working PBS has a great influence on the biosensor because the activity of the immobilized SNA protein may be influenced by the acidity or alkaline of the solution. To optimize the pH, various concentrations have been prepared to test the biosensor by the amperometric *i–t* curve. Fig. 5B shows that ΔI values increase from pH 5.5 and reach maximum values at pH 7.4 prior to decreasing to pH 8.0. Therefore, in the present study, the working PBS (pH=7.4) was chosen as the optimal buffer solution.

The effect of SNA concentration (0.1–1.5 μg mL^{-1}) on the bioreaction efficiency was investigated (Fig. 5C). A significant increase of ΔI values was observed between 0.1 and 1.0 μg mL^{-1} of SNA, while insignificance differences were obtained for greater concentrations. Accordingly, 1.0 μg mL^{-1} of SNA was used for electrode modification.

The influence of incubation time on the reaction of the SNA and Neu5Acα(2-6)Gal β MP Glycoside was significant. As shown in Fig. 5D, ΔI values of the biosensor increased greatly with the increase in incubation time. When the incubation time was over 120 min, ΔI values of the biosensor slightly decreased, suggesting that the amount of Neu5Acα(2-6)Gal β MP Glycoside captured on the surface of the biosensor was saturated. Therefore, the chosen optimal incubation time was 2 h.

3.4. Analytical performance of the biosensor

The amperometric *i–t* curve investigated the performance of the fabricated biosensor under optimized conditions. The current change was directly related to the amount of Neu5Acα(2-6)Gal β MP Glycoside captured on the electrode surface. Fig. S3 displayed typical amperometric *i–t* curve detection of Neu5Acα(2-6)Gal β MP Glycoside with the presence of H_2O_2 and glucose. With an increasing concentration of Neu5Acα(2-6)Gal β MP Glycoside in the range of 0.01 pg mL^{-1}–800 ng mL^{-1}, the increasing amount of bioconjugates formed on the biosensor, resulting in gradual enhanced hindering of electrocatalytic activity. Thus, the electrocatalytic current response decreased. Fig. 5E shows the linear relationship between the current change toward the Neu5Acα(2-6) Gal β MP Glycoside concentrations. The linear regression equation was Y (μA)=10.9598 − 0.8025 ln C with a correlation coefficient (R) of −0.9943. The detection limit was estimated to be 0.003 pg mL^{-1} at a signal to noise ratio of 3σ (where σ is the standard deviation of the blank). A comparison of the detection methods and detection limit between the proposed biosensor and some other reported researches is provided in Table S1, which indicates that the biosensor enabled a relatively low detection limit to be achieved. This result may be based on exploiting AuPt–PPy as the efficient biomimetic catalyst, and GOx may enhance the electrochemical signal by the efficient catalysis of glucose. Furthermore, compared with the other methods, the biocompatibility scaffold film of the proposed biosensor was easier to prepare by one-step synthesis.

3.5. Selectivity, reproducibility and stability of the biosensor

To test further the non-specific absorption of the other biological molecules on the biosensor, control experiments were performed. The current change of the biosensor was recorded, and the results are depicted in Fig. 5F. Firstly, the biosensor was incubated with 1 μg mL^{-1} of high sensitivity C-reaction protein (hs-CRP), beta-galactoside alpha2, 6 sialytransferase (ST6GAL1), L-cysteine, boviene serum albumin (BSA), glucose (Glu), and ascorbic acid (AA). Almost no signal change (ΔI) was observed compared with the blank solution. Furthermore, compared with the current change observed with the 1 ng mL^{-1} Neu5Acα(2-6)Gal β MP Glycoside obtained from mixing these interfering substances, no significant difference was found. The results suggest that the selectivity of the biosensor was acceptable. The specificity of the biosensor is also a key factor in its application. The control experiments have been conducted with and without SNA modification for the detection of Neu5Acα(2-6)Gal β MP Glycoside. The result in Fig. S4A indicate that the proposed biosensor possess a good specificity and was specific to α2,6-sialylated glycans.

To illustrate the reproducibility of the biosensor, a series of five electrodes were used for the detection of 5 ng mL^{-1} Neu5Acα(2-6) Gal β MP Glycoside. The relative standard deviation (RSD) of was 5.3%. This finding demonstrated that the proposed biosensor displayed good reproducibility. The stability of the proposed biosensor was determined by the amperometric *i–t* curve measuring the current change daily during a 7 days period of storage at 4 °C. After 7 days, the result indicated that there was no significant change, and it retained 87.42% of its initial response (Fig. S4B). Obviously, the result shows good long-term stability for the biosensor, which might be attributed to the good biocompatibility of AuPt–PPy and SNA.

3.6. Application in analysis of serum samples

To examine the applicability of the present electrochemical biosensor to biological samples, the biosensor was used to test the recoveries of three concentrations of Neu5Acα(2-6)Gal β MP Glycoside in human serum samples. The serum samples were collected from the Affiliated Hospital of ChongQing Medical University (ChongQing, China). The concentrations (0.5, 5, 800 ng mL^{-1}) of Neu5Acα(2-6)Gal β MP Glycoside spiked human serum samples were prepared by a standard addition method. The results are shown in Table 1, and the ranges of the recovery and the relative standard deviations were 103.32–105% and 3.44–4.94%, respectively. Therefore, the proposed biosensor could be applicable for the analysis of Neu5Acα(2-6)Gal β MP Glycoside in real serum samples

4. Conclusions

To achieve the construction of a simple and low-cost analytical method, for the first time, a novel label-free biosensor was

Table 1
Recovery of serum samples for the electrochemical biosensor using amperometric *i–t* curve analysis (n=3).

Samples	$C_{analyte}$	Added	Found[a]	Recovery	RSD (%)
Sample-1	NT	0.5 pg mL^{-1}	0.52 pg mL^{-1}	103.32	3.75
Sample-2	NT	5 ng mL^{-1}	5.25 ng mL^{-1}	105	3.44
Sample-3	NT	800 ng mL^{-1}	836.49 ng mL^{-1}	104.56	4.94

Samples (1–3) were from healthy people; "NT"represents not detectable.

[a] The values shown here are the average values from three measurements.

developed using AuPt–PPy modified GCE as the sensor platform and GOx for signal enhancement. In this study, AuPt–PPy was successfully synthesized by a facile one-pot reaction, and the nanocomposite exhibited high electrocatalytic activity toward the reduction of H_2O_2. Subsequently, GOx could be employed to block the non-specific sites of the electrode surface and could notably enhance the electrochemical signal by the efficient catalysis of glucose. The fabricated biosensor exhibited remarkable analytic performance, including a wide linear range, a low detection limit, a rapid response and a high sensitivity toward the detection of α2,6-sialylated glycans, because of co-catalysis effects of GOx and AuPt–PPy. This simple technique may have potential application for other biomarkers.

Acknowledgments

This study was supported financially by the National Natural Science Foundation of China (81370403, 21205146).

Appendix A. Supplementary material

Supplementary data associated with this article can be found in the online version at http://dx.doi.org/10.1016/j.bios.2015.10.060.

References

Ahuja, T., Mir, I.A., Kumar, D., Rajesh, 2007. Biomaterials 28, 791–805.
Bai, L., Yuan, R., Chai, Y., Yuan, Y., Zhuo, Y., Mao, L., 2011. Biosens. Bioelectron. 26, 4331–4336.
Bratosin, D., Palii, C., Moicean, A.D., Zanetta, J.P., Montreuil, J., 2007. Biochimie 89, 355–359.
Bugla-Ploskonska, G., Rybka, J., Futoma-Koloch, B., Cisowska, A., Gamian, A., Doroszkiewicz, W., 2010. Microb. Ecol. 59, 601–613.
Cao, H., Yang, D.P., Ye, D., Zhang, X., Fang, X., Zhang, S., Liu, B., Kong, J., 2015. Biosens. Bioelectron. 68, 329–335.
Cao, X., Wang, N., Jia, S., Guo, L., Li, K., 2013. Biosens. Bioelectron. 39, 226–230.
Cete, S., Yasar, A., Arslan, F., 2007. Artif. Cells Blood Substit. Immobil. Biotechnol. 35, 607–620.
Che, X., Yuan, R., Chai, Y., Li, J., Song, Z., Li, W., Zhong, X., 2011. Colloids Surf. B: Biointerfaces 84 (2), 454–461.
Chen, K.J., Chandrasekara Pillai, K., Rick, J., Pan, C.J., Wang, S.H., Liu, C.C., Hwang, B.J., 2012. Biosens. Bioelectron. 33, 120–127.
Chen, S., Zheng, T., Shortreed, M.R., Alexander, C., Smith, L.M., 2007. Anal. Chem. 79, 5698–5702.
Cozzi, P.G., 2004. Chem. Soc. Rev. 33, 410–421.
Dall'Olio, F., Chiricolo, M., Lau, J.T., 1999. Int. J. Cancer 81, 243–247.
Gao, L., He, J., Xu, W., Zhang, J., Hui, J., Guo, Y., Li, W., Yu, C., 2014. Biosens. Bioelectron. 62, 79–83.
Gomes-Filho, S.L.R., Dias, A.C.M.S., Silva, M.M.S., Silva, B.V.M., Dutra, R.F., 2013. Microchem. J. 109, 10–15.
Harduin-Lepers, A., Vallejo-Ruiz, V., Krzewinski-Recchi, M.A., Samyn-Petit, B., Julien, S., Delannoy, P., 2001. Biochimie 83, 727–737.
Hobb, R.I., Tzeng, Y.L., Choudhury, B.P., Carlson, R.W., Stephens, D.S., 2010. Microbes Infect. 12, 476–487.
Hu, W., Li, C.M., Dong, H., 2008. Anal. Chim. Acta 630, 67–74.
Jones, C., 2005. J. Pharm. Biomed. Anal. 38, 840–850.
Kim, J.S., Laskowich, E.R., Michon, F., Kaiser, R.E., Arumugham, R.G., 2006. Anal. Biochem. 358, 136–142.
Lee, J.W., Serna, F., Schmidt, C.E., 2006. Langmuir 22, 9816–9819.
Lin, M., Hu, X., Ma, Z., Chen, L., 2012. Anal. Chim. Acta 746, 63–69.
Li, Y., He, J., Xia, C., Gao, L., Yu, C., 2015. Biosens. Bioelectron. 70, 392–397.
Matsumoto, A., Sato, N., Kataoka, K., Miyahara, Y., 2009. J. Am. Chem. Soc. 131, 12022–12023.
Park, J.J., Yi, J.Y., Jin, Y.B., Lee, Y.J., Lee, J.S., Lee, Y.S., Ko, Y.G., Lee, M., 2012. Biochem. Pharmacol. 83, 849–857.
Pousset, D., Piller, V., Bureaud, N., Monsigny, M., Piller, F., 1997. Cancer Res. 57, 4249–4256.
Raman, R., Raguram, S., Venkataraman, G., Paulson, J.C., Sasisekharan, R., 2005. Nat. Methods 2, 817–824.
Recchi, M.A., Hebbar, M., Hornez, L., Harduin-Lepers, A., Peyrat, J.P., Delannoy, P., 1998. Cancer Res. 58, 4066–4070.
Rover Junior, L., de Oliveira Neto, G., Roberto Fernandes, J., Tatsuo Kubota, L., 2000. Talanta 51, 547–557.
Shoji, E., Freund, M.S., 2002. J. Am. Chem. Soc. 124 (42), 12486–12493.
Wang, P.H., Lee, W.L., Lee, Y.R., Juang, C.M., Chen, Y.J., Chao, H.T., Tsai, Y.C., Yuan, C.C., 2003. Gynecol. Oncol. 89, 395–401.
Wang, W., Gao, Y., Jia, X., Xi, K., 2013. J. Colloid Interface Sci. 396, 23–28.
Zheng, D., Wang, Q., Gao, F., Wang, Q., Qiu, W., Gao, F., 2014. Biosens. Bioelectron. 60, 167–174.
Zhang, M., Yuan, R., Chai, Y., Li, W., Zhong, H., Wang, C., 2011. Bioprocess Biosyst. Eng. 34 (9), 1143–1150.
Zhou, Y., Dong, H., Liu, L., Liu, J., Xu, M., 2014. Biosens. Bioelectron. 60, 231–236.